NANO LETTERS

Letter

pubs.acs.org/NanoLett

Morphological Evolution of Si Nanowires upon Lithiation: A First-Principles Multiscale Model

Ekin D. Cubuk,[†] Wei L. Wang,[†,‡] Kejie Zhao,[†] Joost J. Vlassak,[†] Zhigang Suo,[†] and Efthimios Kaxiras*[,†,‡]

[†]School of Engineering and Applied Sciences and [‡]Department of Physics, Harvard University, Cambridge, Massachusetts 02138, United States

ABSTRACT: Silicon is a promising anode material for high-capacity Li-ion batteries. Recent experiments show that lithiation of crystalline silicon nanowires leads to highly anisotropic morphologies. This has been interpreted as due to anisotropy in equilibrium interface energies, but this interpretation does not capture the dynamic, nonequilibrium nature of the lithiation process. Here, we provide a comprehensive explanation of experimentally observed morphological changes, based on first-principles multiscale simulations. We identify reaction paths and associated structural transformations for Li insertion into the Si {110} and {111} surfaces and calculate the relevant energy barriers from density functional theory methods. We then perform kinetic Monte Carlo simulations for nanowires with surfaces of different orientations, which reproduce to a remarkable degree the experimentally observed profiles and the relative reaction front rates.

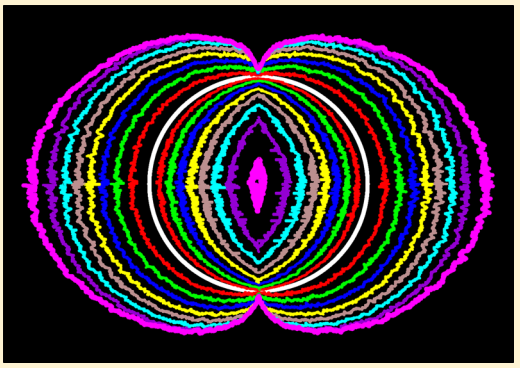

KEYWORDS: *Li-ion batteries, silicon, anisotropy, first-principles*

Increasing the capacity of Li-ion batteries represents a major challenge and the focus of much recent activity in energy storage technology.[1,2] Silicon has attracted intense interest as a promising anode material due to its high theoretical capacity.[3−7] Upon lithiation, the Si anode can swell by a large factor (up to 3−4),[3] which often leads to fracture and limits its application to commercial batteries.[3−5,8,9] Determining the atomic-scale mechanisms associated with this volumetric expansion is crucial in controlling such effects and in designing viable structures for applications. The volume expansion during initial lithiation of crystalline Si (c-Si) is highly anisotropic[10−13] with the ⟨110⟩ orientation growing at a much faster rate than other low-index orientations that cause stress concentration and fracture in certain directions. Experiments also indicate that the lithiation reaction front (RF) is atomically sharp (∼1 nm)[11,14] and progresses linearly with time.[11]

In earlier work, we proposed that the observed anisotropic morphologies are caused by the difference in reaction rates for different crystallographic orientations.[15] The Si surfaces of various orientations have different atomic structures, which lead to distinct lithiation rates; the observed morphologies can be reproduced by continuum models based on reaction rates inferred from experiments.[15−17] Using first-principles calculations, several groups investigated the characteristics of Li insertion into c-Si, but the reaction mechanism involving the progression of the sharp RF was not considered in these studies.[18−22] In an attempt to rationalize the experimentally observed behavior, two different groups[23,24] have recently studied the energetics of equilibrium structures at the {110}, {111}, and {100} interfaces between c-Si and amorphous silicon (a-Si), showing that the first of these interfaces is significantly more stable than the other two. However, since lithiation of Si is a nonequilibrium process, thermodynamically stable states are not expected to form during lithiation.[23,25−27] Accordingly, arguments based on relative energies of equilibrium structures cannot capture the essence of the observed behavior; instead, kinetic rates and the dynamic evolution of the structure are crucial for understanding the lithiation process.

In the present study, we provide a detailed atomistic picture on the lithiation reaction on the {110} and {111} surfaces of c-Si using a multiscale approach based on first-principles and kinetic Monte Carlo (kMC) simulations. We chose those two particular orientations since they represent the fastest and slowest moving surfaces of c-Si upon lithiation and because detailed experimental information is available about growth of Si nanowires with surfaces of these orientations. We identified the reaction paths and the associated structural transformations for the two orientations. The calculated energy barriers for the lithiation reactions indicate that lithiation rates are highly anisotropic, and that there exists a sharp RF for both orientations. We performed kMC simulations that allow us to study the dynamic evolution of a system with such surfaces for much larger scales, both spatial and temporal, than the atomic scale. This made it possible to extract information that can be directly compared to experimental results in a quantitative manner. Our results indicate that the RF for both surfaces

Received: January 11, 2013
Revised: March 22, 2013
Published: March 29, 2013

   dx.doi.org/10.1021/nl400132q | *Nano Lett.* 2013, 13, 2011−2015

progresses linearly with time, its speed in the ⟨110⟩ orientation being 7 times faster than that in ⟨111⟩. The relative lithiation rates,[11,17] the thickness of the RF,[11,17,28] and the anisotropic growth patterns[10,11,26] we obtained are all in excellent agreement with the experimental observations. The present study provides unique insight into the mechanisms of lithiation and morphological evolution of c-Si from a fundamental perspective and highlights the importance of kinetic rates for modeling these nonequilibrium processes. To our knowledge, it is the first attempt to address the problem from a direct and consistent dynamic point of view, which is in contrast with earlier work[23,24] that has relied mainly on equilibrium considerations.

The first-principles calculations within density functional theory were carried out using the SIESTA code[29] with the PBE exchange-correlation functionals. The RFs for the {110} and {111} surfaces were modeled by a six-layer slab of Si atoms subject to the presence of the appropriate number of Li atoms above the Si surface with the primitive cell periodicity of each surface plane or with a 2 × 1 surface supercell for reactions that required more degrees of freedom. We used a local-basis set of double-ζ polarized atomic orbitals with an energy cutoff of 70 Ry, which gives a lattice constant for bulk crystalline Si of 5.52 Å, within 2% of the experimental value.[30] The bottom two layers of the slab with the Si dangling bonds passivated by H atoms were kept fixed at their ideal positions, while the rest of the system was allowed to relax; structural relaxations were considered converged when the magnitude of the force on each atom was smaller than 0.01 eV/Å.

The minimum energy paths for the formation of the RF on the {110} and {111} surfaces are obtained by the following procedure: First, we identify the energetically most favorable positions for the Li atoms on the two surfaces; these configurations are labeled "A" in Figure 1a,b for the {110} and {111} surfaces, respectively. On both surfaces, Li atoms prefer to be on the tetrahedral (T_d) sites of the top layer of Si. This is similar to the energetically preferred site for interstitial Li atoms in bulk Si.[30,31] Next, we identify the energetically favorable position for Li atoms below the top layer of Si, in the presence of additional Li atoms on top of the Si surface. The Li atoms below the top layer prefer to be on the T_d sites, similar to the ones above the top Si layer. The energy barrier for insertion is obtained by connecting the two energetically preferred sites (above and below the top layer of Si) by a reaction coordinate along which one Li atom is constrained in the direction along the path, while all other degrees of freedom are allowed to relax. We ensured that the reaction path is continuous and independent of the direction of drag.[32] This approach gives upper bounds for the energy barriers along the reaction paths considered but allows the exploration of reactions with multiple metastable states. Given the large number of configurations that needed to be explored for this study, this approach provided a reasonable balance between accuracy and computational cost. Some of the energy barriers we obtained were already reported by Chan et al.,[23] and our results are generally in good agreement with their values; we compare these barriers in detail later in the text.

On the {110} surface, the top layer of Si loses some of its bonds to the substrate at 50% lithiation, that is, when half of the Li atoms above the top layer of Si have reached the T_d positions below the top Si layer, as seen in the structure labeled "B" in Figure 1a. At this stage, half of the Si−Si bonds between the top layer of Si and the layer below are broken, a process to which

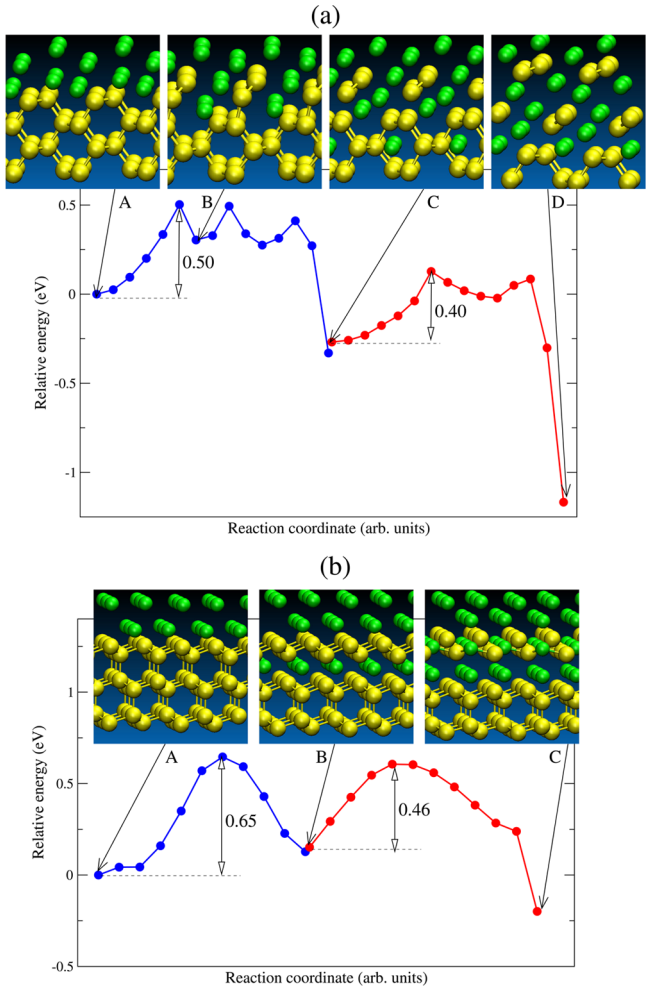

Figure 1. Lithiation process on (a) the {110} Si surface and (b) the {111} surface (green spheres represent Li and yellow spheres Si atoms). The initial, intermediate, and final structures that result in removal of the top Si layer are shown in each case with the relevant energy barriers for the first (blue) and second (red) halves of the process (see text for details).

we refer as the top layer of Si being "peeled-off". We performed similar simulations with a 2 × 1 surface supercell to allow additional degrees of freedom for the lithiation reaction, and obtained the same result, that is, the onset of peeling-off occurs at 50% lithiation. This reaction has an energy barrier of 0.50 eV, which is in good agreement with a previous study.[23] Following this initial stage, half of the Li atoms saturating the surface dangling bonds move to fill the voids created in the T_d positions above the top layer, a process that involves a small (0.13 eV) energy barrier. We replenish the Li atoms to saturate the surface dangling bonds of Si, since in the experimentally relevant situation there is a constant supply of Li atoms above the Si surface. At this point the lithiation process has led to the transformation of the entire first layer of Si atoms into zigzag chains, which are weakly bound to the remaining Si surface, as shown in the configuration labeled "C" of Figure 1a. The curve for the energy barriers relevant to this portion of the reaction is shown in blue in Figure 1a.

One possible scenario is to continue the lithiation reaction from the top of the surface in a similar sequence of steps. The next step of this reaction process has a large barrier of 0.84 eV. However, a much more likely scenario is to have a Li atom

dx.doi.org/10.1021/nl400132q | Nano Lett. 2013, 13, 2011−2015

diffuse into the second layer below the surface from the side. Since this involves motion of a Li atom from a neighboring unit cell, we used the 2 × 1 supercell to calculate its energy barrier, which we found to be 0.50 eV, equal to the energy barrier for bulk diffusion. There are two possibilities for this Li atom to arrive at the desired site for the continuation of the insertion reaction: the first is that it has been inserted with a similar energy barrier from nearby steps on the surface; the second is that it has entered the flat surface at another location, then diffused to the next layer below and reached the reaction location through bulk diffusion. The second scenario involves yet another energy barrier, which corresponds to the Li atom one layer below the surface diffusing to the next layer down. We find this energy barrier to be 0.58 eV, which is somewhat larger than the first barrier of 0.50 eV, but much smaller than the 0.84 eV barrier of the second direct insertion. Previous work has also found this barrier to be larger than the first barrier with slightly different initial configurations.[23] Both of these pathways with the additional 0.50 and 0.58 eV energy barriers, respectively, were included in the kMC simulation.

The second half of the RF formation on the {110} surface is shown by the red curve in Figure 1a. It starts with one of the two T_d positions being filled in both the first and the second layer below the surface, as seen in the structure labeled "C" in Figure 1a. The T_d positions that are occupied by Li atoms on the first and the second layer are the same as far as the local environment is concerned. The next reaction, which has an energy barrier of 0.40 eV, is for the Li atom in the second layer below the surface to move to the other available nearby T_d position. This leads to the second layer beginning to peel-off, which in turn removes the top layer completely in the form of zigzag chains. The two peeled-off layers constitute the RF, with the layers below still having full crystalline order and the Li concentration below the surface being low, as our kMC simulations confirm. We assume that the lifted top layer is easily broken up and incorporated into the amorphous Li_xSi structure and does not influence the further progression of the RF. The final configuration labeled "D" in Figure 1a is very similar to the one labeled "C" with the top layer having been removed, and the RF can propagate through a sequence of similar steps that involve barriers of 0.40 eV for the step from C to D, or 0.50 eV for diffusion steps that bring additional Li atoms into the desired subsurface positions. In summary, for the {110} surface we have identified a process based on atomic-scale steps through which the RF can form and propagate, with the largest energy barrier encountered in this process being 0.50 eV.

On the {111} surface, the corresponding energy barrier from 0 to 50% lithiation below the top layer is 0.65 eV, significantly higher than that on the {110} surface; this is shown in Figure 1b, by the configurations labeled "A" and "B" and the curve for the energy barriers for this portion of the process is shown in blue. Previous work has also reported the barrier for Li insertion into the {111} surface to be much higher than for the {110} surface. The first barrier reported by Chan et al.[23] is actually over 0.80 eV, considerably higher than the value we have found. The difference is most likely due to the different initial conditions assumed in the two calculations. Specifically, we saturated the dangling Si bonds at the top layer with Li atoms and in general made sure that there were enough Li atoms present above the c-Si surface at each stage. This is physically plausible, since the Li atoms diffuse much faster in the amorphous shell than the propagation of the RF, thus they are in high concentration in the neighborhood of the RF. The Si atoms at the top layer are strongly bonded to each other at 50% lithiation below the top layer, which is in contrast to what takes place on the {110} surface. We verify this further using a 2 × 1 surface supercell, which shows that the top layer of Si is not lifted off even at 75% lithiation. The top layer of Si lifts off when 100% of the T_d positions below the top layer are occupied by Li atoms. Similar to {110} case, the second Li atom inserted from the top encounters a large energy barrier (1.1 eV). A much more likely reaction path is to bring the second Li atom from below, through diffusion from the second layer up to the first layer. This is a physically plausible scenario, since the bulk diffusion energy barrier for Li atoms is much lower than the reaction energy barrier on this surface; thus, it is much easier for Li atoms that have already reacted into crystalline Si from steps or other surface facets to diffuse in the bulk until they reach the desired positions for the reaction to proceed. This leads to all the T_d positions being occupied below the top layer of Si, which in turn lifts off this layer as shown in the configuration labeled "C" in Figure 1b; again, the curve for the energy barriers that involve the second Li atom that arrives through subsurface diffusion is shown in red. Unlike the case of the {110} surface, where the lifted Si atoms were in zigzag chains, the {111} layers lift-off as full layers. This has been previously reported[23] as an energetically favorable breaking of the {110} and {111} surfaces. Note that after the top layer of Si is lifted, since the Si atoms diffuse easily through the amorphous shell, the system is identical to the starting position, that is, configurations A and C are equivalent, with the first layer having been removed.

From this analysis, we conclude that the different energy barriers on the {111} and {110} surfaces lead to very anisotropic reaction rates. The limiting energy barrier is 0.65 eV for the {111} surface and 0.50 eV for the {110} surface. Chan et al.[23] have claimed that the anisotropic insertion rates cannot account for the observed anisotropy in growth morphology because even though the energy barrier for insertion into the first layer is lower for {110} the energy barrier for insertion into the second layer from the first layer is not. For the formation and the propagation of the RF, an adequate amount of Li needs to accumulate near the surface to break the Si−Si bonds immediately below the surface. The fact that it is harder for Li to move deeper into the crystal (0.58 eV barrier) than to enter the crystal in the first place (0.50 eV) means that it will accumulate just below the surface, which leads to faster breaking of surface Si−Si bonds. In the picture developed here, this is precisely the reason why the RF moves faster along the ⟨110⟩ direction, since Li atoms enter into Si relatively easily and then mostly accumulate near the top until the top layer is broken off. In contrast to this, along the ⟨111⟩ direction it is considerably more difficult for Li atoms to enter Si (0.65 eV barrier), and the ones that do are more likely to diffuse away into the bulk (0.50 eV) before enough Li accumulates to break off the Si−Si bonds at the top. This picture of the dynamic evolution of the interface and the strong anisotropy of the process on the {110} and {111} surfaces is markedly different than the explanations offered in the other studies,[23,24] which are based on differences in equilibrium structures.

To verify these arguments we setup a kMC simulation[33,34] based on the reaction rates calculated above with a constant pre-exponential factor of 10^{13}. We assume that there are always Li atoms available above the Si crystal on both surfaces. This

dx.doi.org/10.1021/nl400132q | Nano Lett. 2013, 13, 2011−2015

assumption is valid since this system is known to be reaction limited.[15,16] The Li atoms diffuse through the amorphous shell much faster and most of the time is spent waiting for the insertion of Li atoms into the Si crystal. In addition, once a layer of Si is lifted off, it is removed from further consideration assuming it becomes part of the amorphous Li_xSi shell. A layer of the {111} surface is lifted when all four T_d positions below the surface are occupied and a layer of the {110} surface is lifted when half of the T_d positions are occupied on each of the top two layers with alternating positions (the zigzag formation). These choices are a direct consequence of the atomic scale mechanisms identified above, that is, on the {110} surface the RF is formed by 50% lithiation of the two layers below the top layer while on the {111} surface the RF is formed by more than 75% lithiation below the top layer. Near the RF, all energy barriers are considered individually for each surface, depending on the layer, direction, and the occupation of the neighboring T_d positions. Away from the RF, deep in the bulk, the bulk diffusion energy barrier (0.50 eV) is used for both cases. Figure 2 shows the results of the kMC simulation. The RF progresses

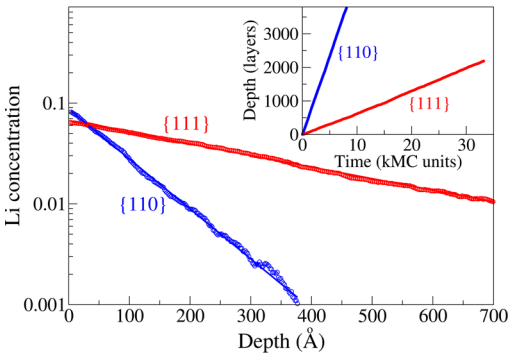

Figure 2. Li concentration depth profile on the {110} and {111} surfaces of Si. The inset shows the depth that the RF has reached as a function of time for the two orientations.

linearly with time in both directions (inset of Figure 2) and moves 7 times faster along the ⟨110⟩ direction than the ⟨111⟩ direction. This result is in good agreement with experiments.[11,17] The Li concentration profile as a function of depth below the surface is calculated by taking a time average of the ratio of T_d positions occupied by Li atoms. Some Li atoms diffuse into the Si bulk after insertion but their concentration is very low. From the balance of diffusion and reaction rates, the distribution of Li atoms in the bulk falls much faster for the {110} surface where the RF is moving fast than for the {111} surface where the RF is moving much slower.

Finally, in order to investigate how the relative propagation speeds of the RF influence the overall growth morphology of Si nanowires we constructed a coarse-grained kMC simulation based on the calculated RF rates. In this model, we assume that the RF propagates 7 times faster along the ⟨110⟩ orientation than along ⟨111⟩ and simulate the lithiation of two Si nanowires with axes along the ⟨112⟩ and the ⟨111⟩ directions, respectively, two representative structures among those that have been studied in experiments.[10,11,13,26,35] In the simulation, we assume that upon lithiation each volume element expands[3] by a factor of 3.5 along the local normal to the surface of the c-Si. For the nanowire with axis along ⟨112⟩, we model the cross sectional surface as a series of {110} and {111} facets, intersecting at right angles as in the ideal crystal. In Figure 3a,

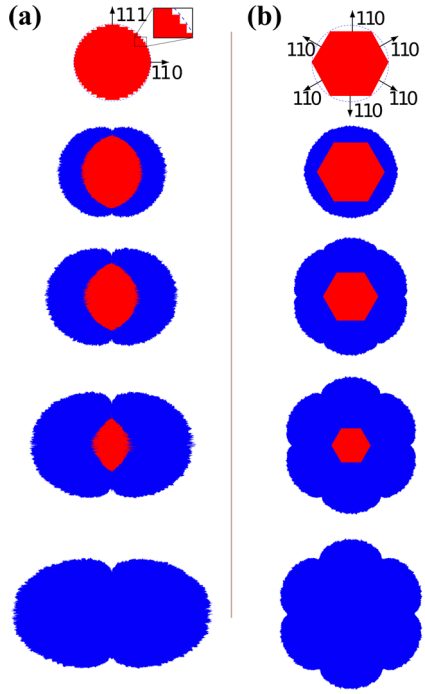

Figure 3. Morphological evolution of the cross sections of SiNWs at different time intervals during lithiation with the inner core of c-Si and the amorphous Li_xSi shell shown in red and blue, respectively. (a) SiNW with axis along ⟨112⟩, modeled as a series of {110} and {111} facets intersecting at right angles. (b) SiNW with axis along ⟨111⟩, modeled as a hexagon with {110} facets.

surfaces facing left and right are in the {110} direction while surfaces facing up and down are in the {111} direction. For the nanowire with axis along ⟨111⟩, we construct the nanowire cross section as a hexagon with {110} facets on all six sides as shown in Figure 3b. The changing morphologies of the nanowires' cross sections are indicated by the color pattern in Figure 3a,b; the inner crystalline Si is shown in red, and the outer lithiated amorphous shell is shown in blue. The overall dumbbell shape of the nanowire with axis along ⟨112⟩ is remarkably similar to experimental observations for wires of this orientation.[11] For the nanowire with axis along ⟨111⟩, the final shape of the lithiated amorphous shell and the progression of the crystalline inner core are also in good agreement with experiments.[10,26] We emphasize that these results involve no adjustable parameters whatsoever, emerging simply from the coarse-grained kMC simulation that is based on the energy barriers described above.

AUTHOR INFORMATION

Corresponding Author

*E-mail: kaxiras@physics.harvard.edu.

Notes

The authors declare no competing financial interest.

ACKNOWLEDGMENTS

This work was supported in part by a grant from the U.S. Army Research Laboratory through the Collaborative Research Alliance (CRA) for Multiscale Multidisciplinary Modeling of Electronic Materials (MSME). We have used the Extreme Science and Engineering Discovery Environment (XSEDE), supported by NSF Grants TG-DMR120073 and TGPHY120021. K.Z., J.J.V., and Z.S. acknowledge support by

the National Science Foundation through a grant on Li-ion Batteries (CMMI-1031161). E.D.C. acknowledges support by the Harvard Graduate Consortium on Energy and Environment Fellowship. W.L.W. acknowledges support from the Massachusetts Green High-Performance Computing Center (MGHPCC).

REFERENCES

(1) Armand, M.; Tarascon, J. M. *Nature* **2008**, *451*, 652−657.
(2) Whittingham, M. S. *MRS Bull.* **2008**, *33*, 411−419.
(3) Kasavajjula, U.; Wang, C. S.; Appleby, A. J. *J. Power Sources* **2007**, *163*, 1003−1039.
(4) Zhang, W. J. *J. Power Sources* **2011**, *196*, 13−24.
(5) Chan, C. K.; Peng, H. L.; Liu, G.; McIlwrath, K.; Zhang, X. F.; Huggins, R. A.; Cui, Y. *Nat. Nanotechnol.* **2008**, *3*, 31−35.
(6) Wen, C. J.; Huggins, R. A. *J. Solid State Chem.* **1981**, *37*, 271−278.
(7) Beaulieu, L. Y.; Hatchard, T. D.; Bonakdarpour, A.; Fleischauer, M. D.; Dahn, J. R. *J. Electrochem. Soc.* **2003**, *150*, A1457−A1464.
(8) Zhao, K. J.; Pharr, M.; Cai, S. Q.; Vlassak, J. J.; Suo, Z. G. *J. Am. Ceram. Soc.* **2011**, *94*, S226−S235.
(9) Beaulieu, L. Y.; Eberman, K. W.; Turner, R. L.; Krause, L. J.; Dahn, J. R. *Electrochem. Solid State Lett.* **2001**, *4*, A137−A140.
(10) Lee, S. W.; McDowell, M. T.; Choi, J. W.; Cui, Y. *Nano Lett.* **2011**, *11*, 3034−3039.
(11) Liu, X. H.; et al. *Nano Lett.* **2011**, *11*, 3312−3318.
(12) Goldman, J. L.; Long, B. R.; Gewirth, A. A.; Nuzzo, R. G. *Adv. Funct. Mater.* **2011**, *21*, 2412−2422.
(13) Lee, S.; McDowell, M.; Berla, L.; Nix, W.; Cui, Y. *Proc. Natl. Acad. Sci. U.S.A.* **2012**, *109*, 4080−4085.
(14) Chon, M. J.; Sethuraman, V. A.; McCormick, A.; Srinivasan, V.; Guduru, P. R. *Phys. Rev. Lett.* **2011**, *107*, 4.
(15) Zhao, K. J.; Pharr, M.; Wan, Q.; Wang, W. L.; Kaxiras, E.; Vlassak, J. J.; Suo, Z. G. *J. Electrochem. Soc.* **2012**, *159*, A238−A243.
(16) Yang, H.; Huang, S.; Huang, X.; Fan, F. F.; Liang, W. T.; Liu, X. H.; Chen, L. Q.; Huang, J. Y.; Li, J.; Zhu, T.; Zhang, S. L. *Nano Lett.* **2012**, *12*, 1953−1958.
(17) Pharr, M.; Zhao, K.; Wang, X.; Suo, Z.; Vlassak, J. J. *Nano Lett.* **2012**, *12*, 5039−5047.
(18) Zhang, Q.; Cui, Y.; Wang, E. *J. Phys. Chem. C* **2011**, *115*, 9376.
(19) Zhang, Q.; Zhang, W.; Wan, W.; Cui, Y.; Wang, E. *Nano Lett.* **2010**, *10*, 3243−3249.
(20) Jung, S.; Han, Y. *Phys. Chem. Chem. Phys.* **2011**, *13*, 21282−21287.
(21) Johari, P.; Qi, Y.; Shenoy, V. B. *Nano Lett.* **2011**, *11*, 5494−5500.
(22) Lv, H.; Jiang, H.; Liu, H.; Shi, J. *J. Appl. Phys.* **2012**, *112*, 103509−103509.
(23) Chan, M. K. Y.; Wolverton, C.; Greeley, J. P. *J. Am. Chem. Soc.* **2012**, *134*, 14362−14374.
(24) Jung, S. C.; Choi, J. W.; Han, Y.-K. *Nano Lett.* **2012**, *12*, 5342−5347.
(25) Zhao, K.; Tritsaris, G. A.; Pharr, M.; Wang, W. L.; Okeke, O.; Suo, Z.; Vlassak, J. J.; Kaxiras, E. *Nano Lett.* **2012**, *12*, 4397−4403.
(26) Lee, S.; Berla, L.; McDowell, M.; Nix, W.; Cui, Y. *Isr. J. Chem.* **2012**, *52*, 1118−1123.
(27) McDowell, M.; Ryu, I.; Lee, S.; Wang, C.; Nix, W.; Cui, Y. *Adv. Mater.* **2012**, *24*, 6034−6041.
(28) Liu, X.; Wang, J.; Huang, S.; Fan, F.; Huang, X.; Liu, Y.; Krylyuk, S.; Yoo, J.; Dayeh, S.; Davydov, M. S., A.V.; Picraux, S.; Zhang, S.; Li, J.; Zhu, T.; J.Y., H. *Nat. Nanotechnol.* **2012**, *7*, 749−756.
(29) Soler, J. M.; Artacho, E.; Gale, J. D.; Garcia, A.; Junquera, J.; Ordejon, P.; Sanchez-Portal, D. *J. Phys.: Condens. Matter* **2002**, *14*, 2745−2779.
(30) Zhao, K. J.; Wang, W. L.; Gregoire, J.; Pharr, M.; Suo, Z. G.; Vlassak, J. J.; Kaxiras, E. *Nano Lett.* **2011**, *11*, 2962−2967.
(31) Wan, W.; Zhang, Q.; Cui, Y.; Wang, E. *J. Phys.: Condens. Matter* **2010**, *22*, 415501.
(32) Jónsson, H.; Mills, G.; Jacobsen, K. W. *Classical and Quantum Dynamics in Condensed Phase Simulations*; World Scientific: New York, 1998; pp 385−404.
(33) Voter, A. F. *Radiat. Eff. Solids* **2007**, *235*, 1−23.
(34) Bortz, A.; Kalos, M.; Lebowitz, J. *J. Comput. Phys.* **1975**, *17*, 10−18.
(35) Liu, X. H.; Zhang, L. Q.; Zhong, L.; Liu, Y.; Zheng, H.; Wang, J. W.; Cho, J. H.; Dayeh, S. A.; Picraux, S. T.; Sullivan, J. P.; Mao, S. X.; Ye, Z. Z.; Huang, J. Y. *Nano Lett.* **2011**, *11*, 2251−2258.